**Revista de Metalurgia**
October-December 2021, 57 (4), e205
ISSN-L: 0034-8570
https://doi.org/10.3989/revmetalm.205

# Characterization of CP-Titanium produced via binder jetting and conventional powder metallurgy

Osman İyibilgin[a,b,*], Engin Gepek[a,c,d]

[a] Sakarya University, Mechanical Engineering Department, Sakarya-Turkey

[b] Biomaterials, Energy, Photocatalysis, Enzyme Technology, Nano and Advanced Materials, Additive Manufacturing, Environmental Applications and Sustainability Research and Development Group (BIOENAMS) Sakarya University, Sakarya 54187, Turkey

[c] Turkish German University, Mechanical Engineering Department, İstanbul-Turkey

[d] Biomedical, Magnetic and Semiconductor Materials Application & Research Center (BIMAS-RC), Sakarya University, Sakarya 54187, Turkey

(*Corresponding author: ibilgin@sakarya.edu.tr)

Submitted: 21 November 2020; Accepted: 13 October 2021; Available On-line: 30 December 2021

**ABSTRACT:** Titanium (Ti) and its alloys are among the most commonly used materials in biomedical applications. In addition to being biocompatible, these materials have notable low density and high corrosion resistance and mechanical properties. It is difficult or impossible to produce parts with complex geometry using conventional powder metallurgy (PM) method since this method is based on shaping powders under uniaxial forces using molds. Binder Jetting is a kind of additive manufacturing technique that do not need molds to shape powders. This study focuses on comparing the properties of the porous CP-Ti parts produced using PM and Binder Jetting. The parts were sintered for 120 min under Argon atmosphere at 1200 °C. After sintering, approximately 94% and 92% relative density values were achieved in the specimens produced using the PM and the 3D printer, respectively. It was also observed that the sample produced using 25 MPa compacting pressure has a hardness of 317±10 $HV_{0.05}$ and a compressive (yield) strength of 928 MPa while its counterpart produced using the 3D printer has a hardness of 238±8 $HV_{0.05}$ and a compressive (yield) strength of 342 MPa. Although the hardness and strength of the specimens produced with the 3D printer were lower than PM ones, their properties are appropriate for producing implants to replace bone structures.

**KEYWORDS:** Additive manufacturing; Binder jetting; Biomaterials; Porous titanium; Powder metallurgy

Citation/Citar como: İyibilgin, O.; Gepek, E. (2021). "Characterization of CP-Titanium produced via binder jetting and conventional powder metallurgy". *Rev. Metal.* 57(4): e205. https://doi.org/10.3989/revmetalm.205

**RESUMEN:** *Caracterización de CP-Titanio producido mediante inyección aglutinante y pulvimetalurgia convencional.* El titanio (Ti) y sus aleaciones se encuentran entre los materiales más utilizados en aplicaciones biomédicas. Además de ser biocompatibles, estos materiales tienen una baja densidad, una alta resistencia a la corrosión y unas propiedades mecánicas notables. Es muy difícil producir piezas con geometría compleja utilizando métodos convencionales de pulvimetalurgia (PM) ya que este método se basa en dar forma a polvos bajo fuerzas

uniaxiales utilizando moldes. La Inyección Aglutinante (Binder Jetting) es un tipo de técnica de fabricación aditiva que no necesita moldes para dar forma a los polvos. Este estudio se centra en comparar las propiedades de las piezas porosas de CP-Ti producidas con PM e Inyección Aglutinante. Las piezas se sinterizaron durante 120 min en una atmósfera de argón a 1200 °C. Después de la sinterización, se alcanzaron valores de densidad relativa de aproximadamente el 94% y el 92% en las muestras producidas por PM y con la impresora 3D, respectivamente. También se observó que la muestra producida con una presión de compactación de 25 MPa tiene una dureza de 317 ± 10 $HV_{0.05}$ y un límite elástico bajo compresión de 928 MPa, mientras que la pieza producida con la impresora 3D tiene una dureza de 238 ± 8 $HV_{0.05}$ y un límite elástico bajo compresión de 342 MPa. Aunque la dureza y resistencia de las muestras producidas con la impresora 3D fueron menores que las de PM, sus propiedades son adecuadas para producir implantes que reemplacen las estructuras óseas.

**PALABRAS CLAVE:** Biomateriales; Fabricación aditiva; Inyección aglutinante; Pulvimetalurgia; Titanio poroso

**ORCID ID:** Osman İyibilgin (https://orcid.org/0000-0002-1288-1920); Engim Gepek (https://orcid.org/0000-0001-7340-8363)

## 1. INTRODUCTION

The high strength/weight ratio, high corrosion resistance and biocompatibility of titanium (Ti) and Ti alloys provide an important role in the aerospace, biomedical, energy, and marine applications (Zadra *et al.*, 2008; Sidambe, 2014; Chen and Thouas, 2015; Yadav *et al.*, 2019). The density and elastic modulus of Titanium (Ti) and Ti alloys, frequently used in biomedical applications, are different from the bone structure. The difference in elastic modulus results in weak osseointegration and stress concentrations at the attachment points of the implant due to the stress shielding effect (Goharian and Abdullah, 2017; Domínguez-Trujillo *et al.*, 2018). Also, high hardness of implant causes bone resorption and shortening of the life of the implant (Frost, 1994). These problems can be minimized by producing porous implants with similar mechanical properties to bone tissue. Porous Ti implants with low density can be manufactured by conventional powder metallurgy method and additive manufacturing techniques (Wiria *et al.*, 2010; Goia *et al.*, 2013; Tojal *et al.*, 2013; Yang *et al.*, 2018; Yılmaz *et al.*, 2018; Castillo *et al.*, 2019).

In conventional powder metallurgy method (PM), the end-user products are obtained by sintering the parts that shaped by applying pressure to the powder material filled into the mold. Although this method is fast and economical to produce a large number of small and uncomplicated parts, the cost and time of production are high for producing complex and low quantity of patient-specific implants. In this method, powder material properties, compression pressure, and sintering conditions directly affect the density and mechanical properties of the final products (Esteban *et al.*, 2011; Castillo *et al.*, 2019; Cuesta *et al.*, 2019).

Binder Jetting (BJ) is an additive manufacturing method invented in 1993 at the Massachusetts Institute of Technology (Stevens *et al.*, 2018). In this method, any type of materials such as polymers, ceramics, metal, and composites can be combined with binders to manufacture parts without using a mold (Karageorgiou and Kaplan, 2005; Sheydaeian and Toyserkani, 2018; Tran *et al.*, 2019). The product can be fabricated directly from the 3D CAD design file with a 3D printer in the BJ method. Not using molds in manufacturing processes makes the fabrication of complex parts easier, more economical, and faster. The density, microstructure, and mechanical properties of the part produced by the 3D printer vary depending on the powder shape, powder size distribution, layer thickness, and the amount of binder used during combining (Mostafaei *et al.*, 2016; Bai and Williams, 2018; Miyanaji *et al.,* 2019).

As it has been presented in this literature survey, many different methods were performed to produce porous CP-Ti samples. Binder jetting and uniaxial pressing have its own advantages and disadvantages. Comparing the microstructural and mechanical properties of CP-Ti parts produced by binder jetting and axial pressing allows us to know more about these two production methods. In this study, the microstructure and mechanical properties of porous Ti parts fabricated by conventional powder metallurgy and binder jetting methods are compared and the effects of the manufacturing method on the microstructure and the mechanical properties were investigated. For this purpose, Ti powders were shaped using these methods and then sintered at 1200 ºC in an atmosphere-controlled furnace.

## 2. MATERIALS AND METHOD

### 2.1. Materials

In this study, commercial -325 mesh titanium powders with 99.5% purity (Alfa Aesar, 42624) were used to manufacture Ti specimens. The size distribution of titanium powders was analyzed using Microtrac s3500 laser diffraction particle analysis system. The sizes of Ti powders were measured d10 = 7.11 µm, d50 = 17.75 µm and d90 = 32.35 µm. The powder size distribution as well as a SEM image of the Ti powders are shown in Fig. 1.

The flow characteristic of powder material can be measured with many methods such as static repose angle, Hausner ratio, mass flow through an orifice,

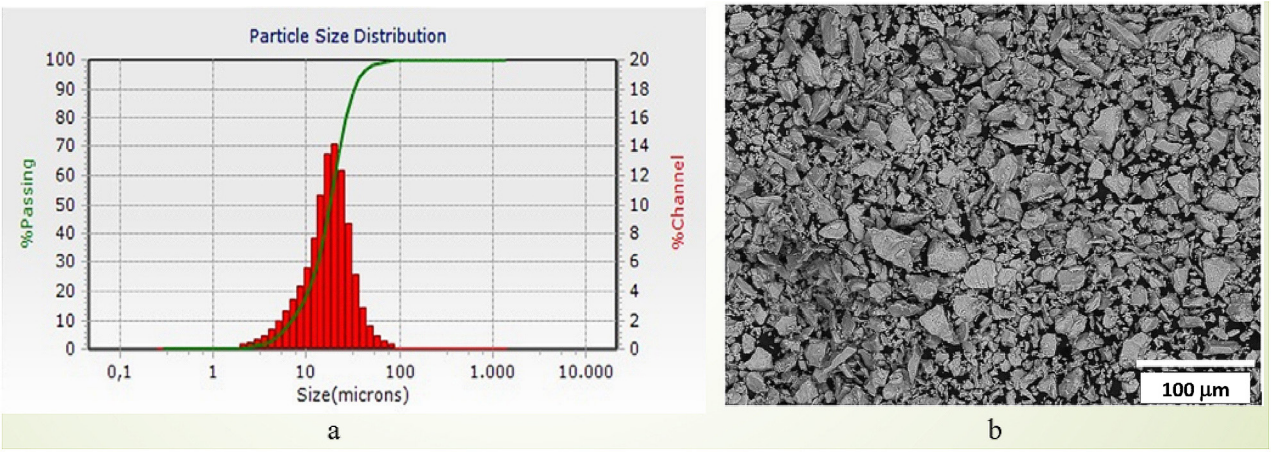


FIGURE 1. Powder properties: a) Powder size distribution of the Ti powder, b) SEM images of Ti powders.

and powder internal cohesion (Amidon, Meyer and Mudie, 2017; Ziaee and Crane, 2019). In this study, flow characteristics of Ti powders were determined as Hausner ratio (tap density over apparent density). Powder materials with a Hausner ratio of less than 1.4 have sufficient flow characteristics (Amidon, Meyer and Mudie, 2017). Table 1 shows that the Hausner ratio of Ti powders was 1.21 which means that Ti powders had acceptable flowability and were suitable for Binder Jetting.

TABLE 1. Properties of Ti particles

| Bulk volume ($mm^3$) | Tapped volume ($mm^3$) | Hausner ratio | $d_{10}/d_{50}/d_{90}$ (µm) |
|---|---|---|---|
| **35** | 29 | 1.21 | 7.11/17.75/32.35 |

## 2.2. Manufacturing of test specimens

Ti test specimens were shaped with a uniaxial pressing (MSE, uniaxial) and a customized Binder jetting 3D printer. Figure 2 shows a schematic of the Binder Jetting process setup. In the uniaxial press method, Ti powders were filled into a mold with a diameter of 10 mm and compacted with a pressure of 25, 100 and, 200 MPa to produce Ti specimens with varied density.

In the Binder Jetting method, cylindrical specimens of diameter 10 mm and height 10 mm were fabricated in a 3D printer with processing parameters as follows: binder saturation of 100%, a layer thickness of 100 µm, binder temperature of 45 °C. HP liquid binder was used in the fabrication of

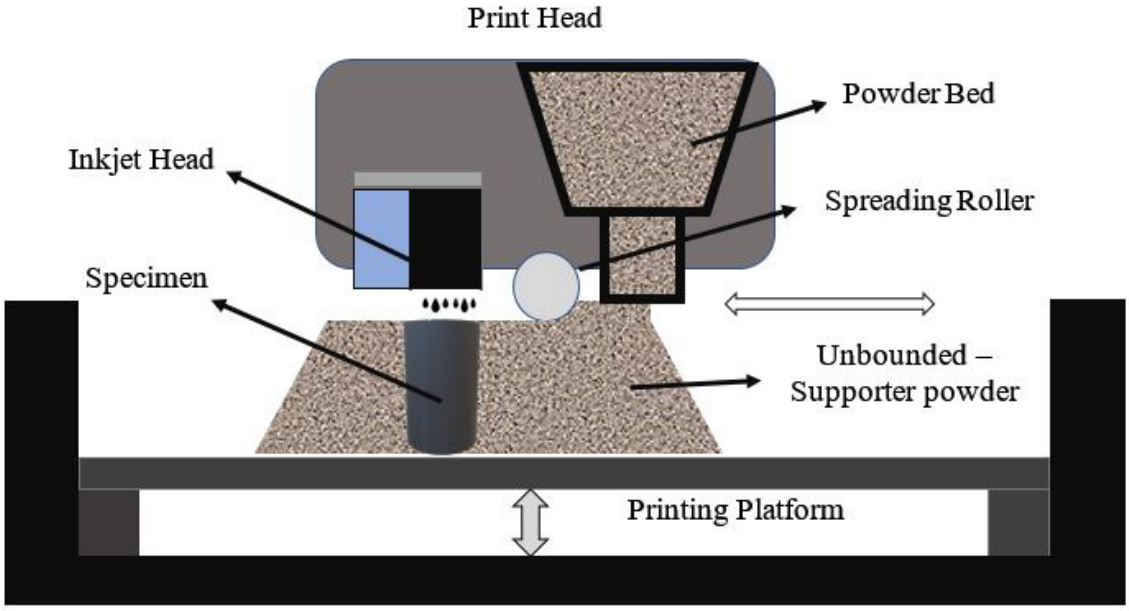


FIGURE 2. Schematic of the Binder Jetting process.

test specimens. During Binder Jetting manufacturing process, the powder material was spread on the powder bed as a thin layer and the binder adhesive was deposited on the top of the powder layer where required. This process was repeated for the second and other layers until the fabrication was completed. After fabrication, the unbound powder materials surrounding the object in the pool were cleaned to obtain green parts.

### 2.3. Sintering

The sintering process was carried out in a High Temperature Tube Furnace (Protherm). Schematic presentation of the sintering cycle for Ti is shown in Fig. 3. Before the sintering process, the binder and space holder were burnout at 250 ºC. Then the furnace was heated at a rate of 5 °C·min$^{-1}$ to the sintering temperature and held isothermally for 2 h. The specimens fabricated by PM, and 3D printer were sintered at 1200 ºC under argon atmosphere.

The relative density of the sintered test specimens was measured by the Archimedes water immersion principle using a balance with 0.0001 g precision. The porosity ratio of the test specimens was calculated using Eq. (1) (P: Porosity ratio, ρ: Measured density of Ti, $\rho_s$: Calculated theoretical density of Ti).

$$P = \frac{1-\rho}{\rho_s} x100 \quad (1)$$

Microstructural analyses of specimens were made after the standard metallographic procedure, which is a grinding sequence of 180, 400, 800, and 1200 grit silicon carbide paper and later polishing on a 1 mm alumina suspension. Microstructures and pore morphologies of Ti test specimens were analyzed using a scanning electron microscope (JEOL brand JSM 6060) and SEM-coupled Energy Distributor Spectrometry (EDS), respectively. SEM images were taken from polished Ti samples. EDS analyses were taken from the area for specimens produced with the PM and 3D printer. In addition, EDS analysis was performed for points 1 and 2 of the BJ-produced samples shown in Fig. 6d. The phase contents of sintered specimens were characterized by XRD (Rigaku D/MAX 2000 X-ray generator and diffractometer) with Cu Kα radiation (1.54059 A°) at a scanning rate of 2 °/min.

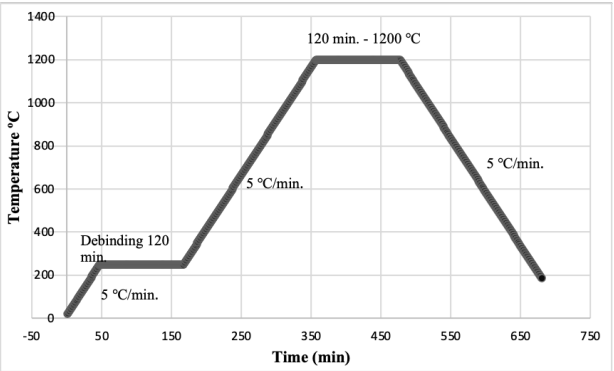


FIGURE 3. Schematic presentation of the sintering cycle for CP-Ti.

Compression and microhardness tests were performed to determine the mechanical properties of the specimens. The microhardness (represented by HV) values of the alloys were measured using a hardness testing apparatus (Wilson 402 MVS, USA) using a load of 50 g for 15 s. A total of 5 measurements were made to determine the hardness of specimens for each test specimens. Compressive tests were performed at room temperature with a Zwick-Roell testing machine at 30 MPa/s loading rate. The compression strengths of the specimens were determined by an average of 3 specimen's compressive tests.

## 3. RESULT AND DISCUSSION

### 3.1. Density and porosity

The relative densities of the sintered test specimens are shown in Table 2. During compacting, the pressure applied to the powder material results in the rearrangement of the particles, deformation, and the hardening of the material to form a solid model (Lemoisson and Froyen, 2005; Križan *et al.*, 2016). In the compacting curve of ceramics and metals, there is a steep increase at first in density and then a slower increase followed by a plateau in density (Francis, 2016). While the relative density of the sample shaped with 25 MPa compacting pressure is 94.32%, the relative density of specimens shaped with 200 MPa compacting pressure increases to 98.19%. A relative density value of 92.63% was obtained in specimens fabricated with a 3D printer without applying pressure. In this study, the density of samples pressed with low compacting pressure is closer to the samples fabricated by 3D printer. In uniaxial pressing, as the compression pressure increased from 25 MPa to 200 MPa, a continuous in-

TABLE 2. Relative densities of test specimens

| Manufacturing Method | Compaction Pressure (MPa) | Relative Density (%) |
|---|---|---|
| **Binder Jetting** | 0 | 92.63 ± 5.6 |
| **Conventional Powder Metallurgy** | 25 | 94.32 ± 2.03 |
| | 100 | 96.86 ± 1.5 |
| | 200 | 98.19 ± 1.2 |

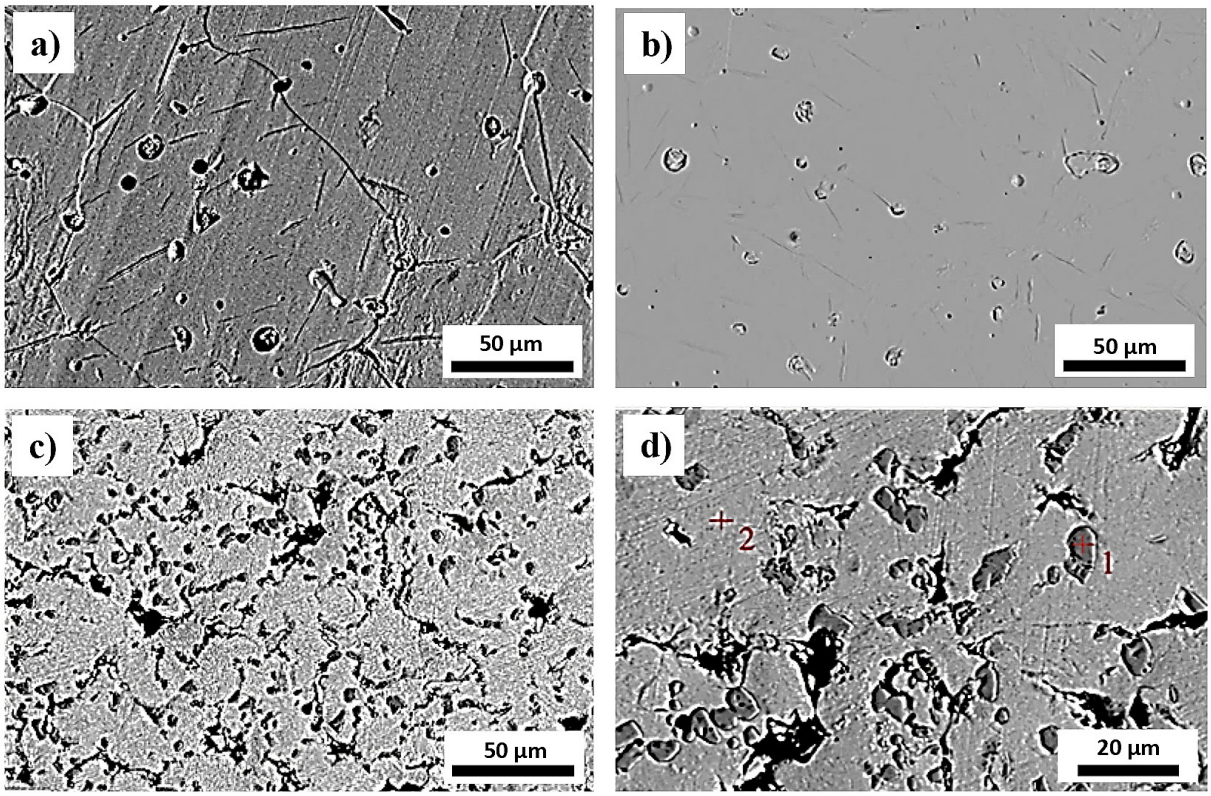


FIGURE 4. SEM images of test specimens: a) 25 MPa, b) 200 MPa, c), d) Binder Jetting.

crease in densities of test samples was observed due to the inter-particle spaces decreased and the particles moved closer to each other.

The SEM images of the Ti specimens fabricated using uniaxial press and 3D printer are shown in Fig. 4. It is observed that pores of the specimens produced with uniaxial press method have a spherical morphology and shrink with the increase of compression pressure. The compression pressure applied to the powder material enables the small irregular pores to combine and hence lead to a reduction of the large-sized pores (Amidon *et al.*, 2017; Castillo *et al.*, 2019). It is seen that the pores of specimens fabricated by 3D printer are non-uniform and exist in different sizes. In the Binder Jetting method, pores are non-uniform due to the lack of compression pressure, the droplet effect of the liquid binder and, the accumulation of binder between particles (Kunchala and Kappagantula, 2018; Stevens *et al.*, 2018; Castillo *et al.*, 2019).

The XRD pattern of Ti- α phase and Ti specimens fabricated by uniaxial press (25 MPa) and BJ are shown in Fig. 5. The diffraction peaks corresponding to Ti-α phase were observed in all the specimens (Balbinotti *et al.*, 2011). EDS analysis graph of the Ti specimens were shown in Fig. 6. XRD and EDS analyzes showed that Ti-α phase is predominant which indicate that there is no a significant amount of impurities in titanium structure.

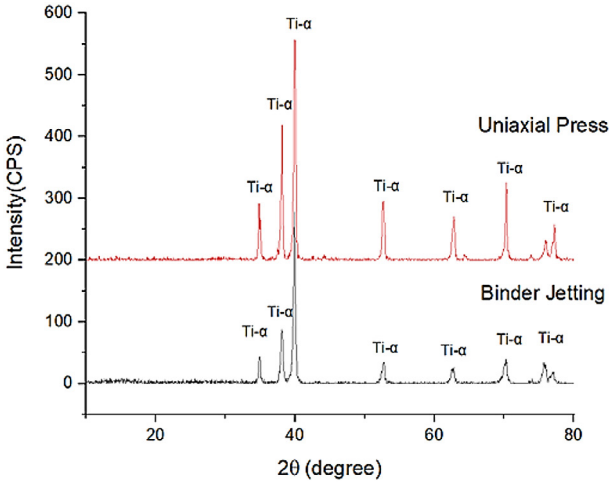


FIGURE 5. XRD patterns of the specimens fabricated by Uniaxial Press (25 MPa; upper diffractogram, in red) and Binder Jetting (lower diffractogram, in black) methods.

### 3.2. Microhardness

Microhardness values of test specimens are shown in Fig. 7. It is clear that the shaping method

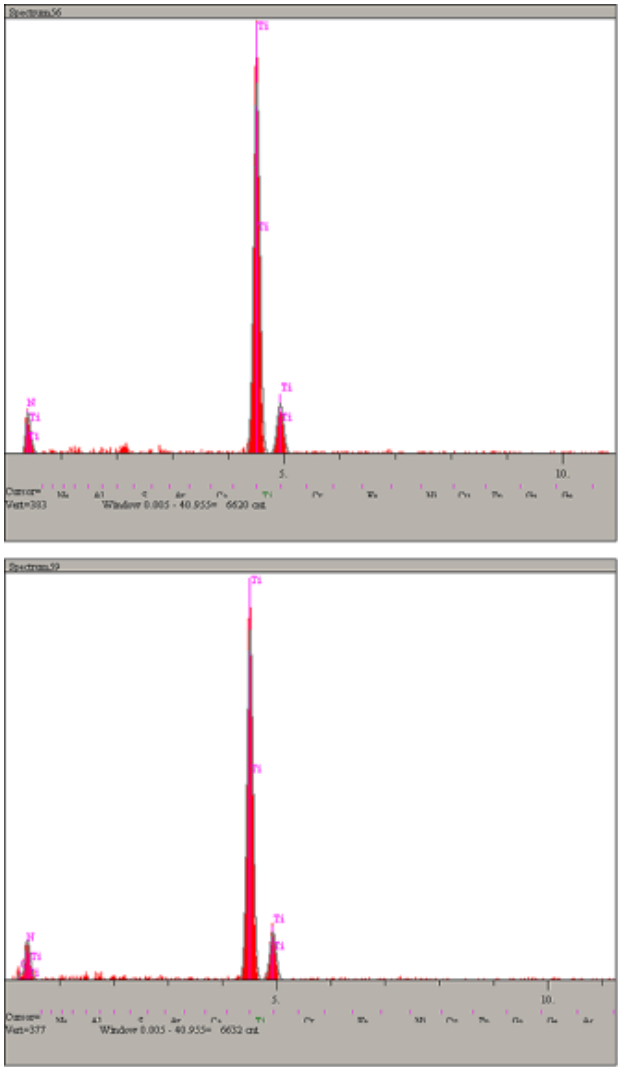

FIGURE 6. EDS analysis results of test specimens: a) Uniaxial Press (25 MPa), b) Binder Jetting.

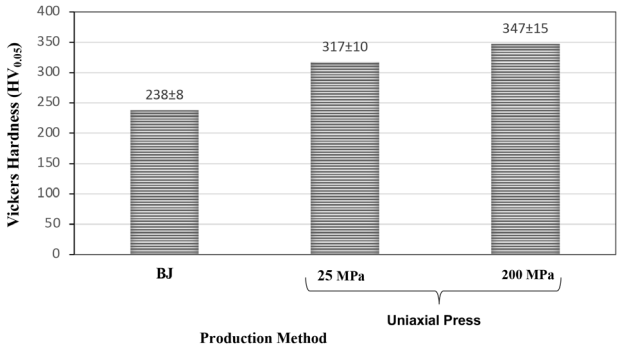


FIGURE 7. Microhardness values of Ti test specimens.

directly affects the microhardness of the structure. The hardness of specimens fabricated with the conventional powder metallurgy increases as the compaction pressure increase. While the microhardness value measured in test specimens produced with 25 MPa compression pressure is 317±10 $HV_{0.05}$, the microhardness value when the compaction pressure increases to 200 MPa is 347±15 $HV_{0.05}$. This increase in microhardness indicates that the microhardness depends on the density and pore sizes (Gagg *et al.*, 2013; Zhao *et al.*, 2019). The hardness values of the specimens produced with 3D printing method without applying pressing were measured as 238±8 $HV_{0.05}$. Although the relative density of the test samples produced with the Binder Jetting method and 25 MPa compression pressure is close to each other, the hardness values of BJ test samples are lower. Previous studies reported similar results that the compacting pressure lead to the increase in densification, hardness and compressive strength (Ryan *et al.*, 2008; Castillo *et al.*, 2019). The hardness of Ti samples, has 97% relative density, fabricated by spark plasma sintering were found as 341.71 HV (Mahundla *et al.*, 2021). In another study, Ti samples spark plasma sintered at 1200 ºC had hardness of 391 HV (Shahedi Asl *et al.*, 2018). The hardness of the Ti samples produced by the 3D printer method and with lower density was found to be 182.8 HV (Xion *et al.*, 2012). These results show that the production method and density directly affect the hardness of Ti samples.

### 3.3. Compressive strength

The compressive (yield) strengths of Ti test specimens are shown in Fig. 8. In previous study the compressive strength of pure Ti produced with 3D binder jetting method was found between 167 to 455 MPa (Wiria *et al.*, 2010). The compressive strength of pure Ti fabricated by selective laser melting (SLM) varies between 235±52 and 1136±15 MPa depending on the porosity ratio (Attar *et al.*, 2015). In conventional powder metallurgy method, when the compression pressure is increased from 25 MPa to 200 MPa, the compressive strength increases from 928±21 MPa to 1154±32 MPa. The increase in compaction pressure causes the decrease of the amount of porosity and pore interconnectivity, resulting in a part with higher compression strength (Križan *et al.*, 2016;

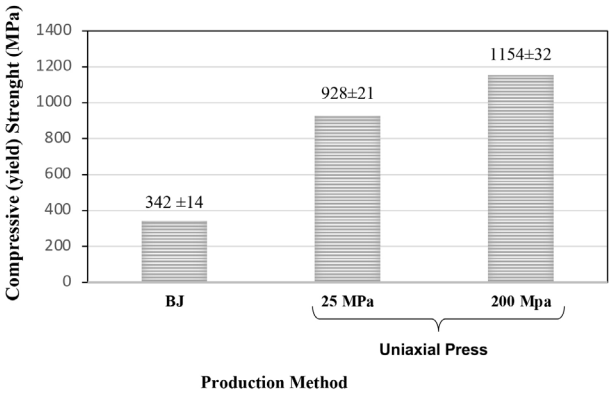


FIGURE 8. Compressive (yield) strength of Ti test specimens.

Mostafaei *et al.*, 2017; Yegyan Kumar *et al.*, 2019). The compressive strength of the Ti pieces produced by the 3D printing method (342 ±14 MPa) resulted in lower values. The main factor in the mechanical properties of the porous materials is the total porosity (Veljović *et al.*, 2011). However, in this study, the specimens with similar total porosity ratios are compared. The more spherical pores and strong spherical agglomerates in the samples produced by axial pressing resulted in better mechanical properties. The irregular pore structures of the specimens produced by BJ method cause lower strength (Križan *et al.*, 2016; Yan *et al.*, 2017). It is seen that the pore morphology affects the mechanical properties. Although the parts produced by 3D printing have lower strength, they are still higher than the strength of the cortical bone (compressive strength 114–195 MPa) (Torres-Sanchez *et al.*, 2017; Yılmaz *et al.*, 2018). Also, with additive manufacturing techniques, more successful results might be obtained in patient-specific biomedical applications (Harun *et al.,* 2018). Compared to many conventional manufacturing methods, additive manufacturing methods provide significant advantages in high-tech applications, orthopedic and dental applications (Avila *et al.*, 2018).

## 4. CONCLUSION

Test specimens were fabricated and sintered by conventional powder metallurgy and 3D printing using commercial CP-Titanium powder. Better mechanical properties are obtained in specimens fabricated by compaction pressure. Although the mechanical strength of the specimens fabricated with a 3D printer are lower, they provide sufficient strength for biomedical applications.

## ACKNOWLEDGE

Thanks to BIMAS-RC due to provision of laboratory facilities. This study was supported by the Sakarya University Scientific Research Projects Foundation with projects numbered as 2017-50-01-044 and 2017-50-01-045.

## REFERENCES

Amidon, G.E., Meyer, P.J., Mudie, D.M. (2017). *Particle, powder, and compact characterization. In Developing Solid Oral Dosage Forms: Pharmaceutical Theory and Practice*. Chapter 10, Second Edition. Elsevier Inc., pp. 271-293. https://doi.org/10.1016/B978-0-12-802447-8.00010-8.

Attar, H., Löber, L., Funk, A., Calin, M., Zhang, L.C., Prashanth, K.G., Scudino, S., Zhang, Y., Eckert, J. (2015). Mechanical behavior of porous commercially pure Ti and Ti-TiB composite materials manufactured by selective laser melting. *Mater. Sci. Eng. A* 625, 350–356. https://doi.org/10.1016/j.msea.2014.12.036.

Avila, J.D., Bose, S., Bandyopadhyay, A. (2018). *Additive manufacturing of titanium and titanium alloys for biomedical applications. In Titanium in Medical and Dental Applications*. Elsevier Inc., pp. 325-343. https://doi.org/10.1016/B978-0-12-812456-7.00015-9.

Bai, Y., Williams, C.B. (2018). The effect of inkjetted nanoparticles on metal part properties in binder jetting additive manufacturing. *Nanotechnology* 29 (39), 395706. https://doi.org/10.1088/1361-6528/aad0bb.

Balbinotti, P., Gemelli, E., Buerger, G., Amin de Lima, S., De Jesus, J., Almeida, N.H., Rodrigues Enriques, V.A., Almeida Soares, G. (2011). Microstructure development on sintered Ti/HA biocomposites produced by powder metallurgy. *Mat. Res.* 14 (3), 384–393. https://doi.org/10.1590/S1516-14392011005000044.

Castillo, S.M., Muñoz, S., Trueba, P., Díaz, E., Torres, Y. (2019). Influence of the Compaction Pressure and Sintering Temperature on the Mechanical Properties of Porous Titanium for Biomedical Applications. *Metals* 9 (12), 1249. https://doi.org/10.3390/met9121249.

Chen, Q., Thouas, G.A. (2015). Metallic implant biomaterials. *Mater. Sci. Eng. R* 87, 1–57. https://doi.org/10.1016/j.mser.2014.10.001.

Cuesta, I.I., Martínez-Pañeda, E., Díaz, A., Alegre, J.M. (2019). Cold isostatic pressing to improve the mechanical performance of additively manufactured metallic components. *Materials* 12 (15), 2495. https://doi.org/10.3390/ma12152495.

Domínguez-Trujillo, C., Ternero, F., Rodríguez-Ortiz, J.A., Heise, S., Boccaccini, A.R., Lebrato, J., Torres, Y. (2018). Bioactive coatings on porous titanium for biomedical applications. *Surf. Coat. Tech.* 349, 584–592. https://doi.org/10.1016/j.surfcoat.2018.06.037.

Esteban, P.G., Bolzoni, L., Ruiz-Navas, E.M., Gordo, E. (2011). Introducción al procesado pulvimetalúrgico del titanio. *Rev. Metal.* 47 (2), 169–187. https://doi.org/10.3989/revmetalmadrid.0943.

Francis, L.F. (2016). *Powder Processes. In Materials Processing.* A Unified Approach to Processing of Metals, Ceramics and Polymers. pp. 343–414. https://doi.org/10.1016/B978-0-12-385132-1.00005-7.

Frost, H.M. (1994). Wolff's Law and bone's structural adaptations to mechanical usage: an overview for clinicians. *Angle Orthod.* 64 (3), 175–188.

Gagg, G., Ghassemieh, E., Wiria, F.E. (2013). Effects of sintering temperature on morphology and mechanical characteristics of 3D printed porous titanium used as dental implant. *Mater. Sci. Eng. C* 33 (7), 3858–3864. https://doi.org/10.1016/j.msec.2013.05.021.

Goharian, A., Abdullah, M.R. (2017). *Bioinert Metals (Stainless Steel, Titanium, Cobalt Chromium). In Trauma Plating Systems*. Biomechanical, Material, Biological, and Clinical Aspects. Elsevier Inc., pp. 115-142. https://doi.org/10.1016/B978-0-12-804634-0.00007-0.

Goia, T.S., Violin, K.B., Bressiani, J.C., De Almeida, A.H. (2013). Titanium and Ti-13Nb-13Zr alloy porous implants obtained by space-holder technique with addition of albumin. *Key Eng. Mater.* 529–530, 574–579. https://doi.org/10.4028/www.scientific.net/KEM.529-530.574.

Harun, W.S.W., Manan, N.S., Kamariak, M.S.I., Sharif, S., Zulkifly, A.H., Ahmad, I., Miura, H. (2018). A review of powdered additive manufacturing techniques for Ti-6al-4v biomedical applications. *Powder Technol.* 331, 74–97. https://doi.org/10.1016/j.powtec.2018.03.010.

Karageorgiou, V., Kaplan, D. (2005). Porosity of 3D biomaterial scaffolds and osteogenesis. *Biomaterials*. 26(27), 5474-5491. https://doi.org/10.1016/j.biomaterials.2005.02.002.

Križan, P., Matúš, M., Beniak, J. (2016). Relationship between compacting pressure and conditions in pressing chamber during biomass pressing. *Acta Polytech.* 56 (1), 33–40. https://doi.org/10.14311/APP.2016.56.0033.

Kunchala, P., Kappagantula, K. (2018). 3D printing high density ceramics using binder jetting with nanoparticle densifiers. *Mater. Design* 155, 443–450. https://doi.org/10.1016/j.matdes.2018.06.009.

Lemoisson, F., Froyen, L. (2005). *Understanding and improving powder metallurgical processes. In Fundamentals of Metallurgy*. Woodhead Publishing Series, pp. 471-502.

https://doi.org/10.1533/9781845690946.2.471.
Mahundla, M.R., Matizamhuka, W.R., Shongwe, M.B. (2021). The effect of densification on hardness of Ti, Ti-6Al-4V, Ti-34Nb-25Zr alloy produced by spark plasma sintering. *Mater. Today* 38 (Part 2), 605-608. https://doi.org/10.1016/j.matpr.2020.03.468.
Miyanaji, H., Momenzadeh, N., Yang, L. (2019). Effect of powder characteristics on parts fabricated via binder jetting process. *Rapid Prototyping Journal* 25 (2), 332–342. https://doi.org/10.1108/RPJ-03-2018-0069.
Mostafaei, A., Stevens. E.L., Hughes, E., Biery, Sh., Hilla, C., Chmielus, M. (2016). Powder bed binder jet printed alloy 625: Densification, microstructure and mechanical properties. *Mater. Design* 108, 126–135. https://doi.org/10.1016/j.matdes.2016.06.067.
Mostafaei, A., Toman, J., Stevens, E.L., Hughes, E.T., Krimer, Y.L., Chmielus, M. (2017). Microstructural evolution and mechanical properties of differently heat-treated binder jet printed samples from gas- and water-atomized alloy 625 powders. *Acta Mater.* 124, 280–289. https://doi.org/10.1016/j.actamat.2016.11.021.
Ryan, G.E., Pandit, A.S., Apatsidis, D.P. (2008). Porous titanium scaffolds fabricated using a rapid prototyping and powder metallurgy technique. *Biomaterials* 29 (27), 3625–3635. https://doi.org/10.1016/j.biomaterials.2008.05.032.
Shahedi Asl, M., Namini, A.S., Motallebzadeh, A., Azadbeh, M. (2018). Effects of sintering temperature on microstructure and mechanical properties of spark plasma sintered titanium. *Mater- Chem. Phys.* 203, 266–273. https://doi.org/10.1016/j.matchemphys.2017.09.069.
Sheydaeian, E., Toyserkani, E. (2018). Additive manufacturing functionally graded titanium structures with selective closed cell layout and controlled morphology. *Int. J. Adv. Manuf. Technol.* 96 (9–12), 3459–3469. https://doi.org/10.1007/s00170-018-1815-2.
Sidambe, A.T. (2014). Biocompatibility of advanced manufactured titanium implants-A review. *Materials* 7 (12), 8168–8188. https://doi.org/10.3390/ma7128168.
Stevens, E., Scholder, S., Bono, E., Schmidt, D., Chmielus, M. (2018). Density variation in binder jetting 3D-printed and sintered Ti-6Al-4V. *Addit. Manuf.* 22, 746–752. https://doi.org/10.1016/j.addma.2018.06.017.
Tojal, C., Amigó, V., Calero, J.A. (2013). Fabricación y caracterización de aleaciones porosas de Ti y Ti6Al4V producidas mediante sinterización con espaciador. *Rev. Metal.* 49 (1), 20–30. https://doi.org/10.3989/revmetalm.1206.
Torres-Sanchez, C., Al Mushref, F.R.A., Norrito, M., Yendall, K., Liu, Y., Conway, P. (2017). The effect of pore size and porosity on mechanical properties and biological response of porous titanium scaffolds. *Mater. Sci. Eng. C* 77, 219–228. https://doi.org/10.1016/j.msec.2017.03.249.
Tran, T.Q., Chinnappan, A., Yoong Lee, J.K., Loc, N.H., Tran, L.T., Wang, G., Kumar, V., Jayathilaka, W., Ji, D., Doddami, M., Ramarkrishna, S. (2019). 3D printing of highly pure copper. *Metals* 9 (7), 12–20. https://doi.org/10.3390/met9070756.
Veljović, Dj., Jančić-Hajneman, R., Balać, I., Jokić, B., Putić, S., Petrović, R., Janaćković, Dj. (2011). The effect of the shape and size of the pores on the mechanical properties of porous HAP-based bioceramics. *Ceramics International* 37 (2), 471–479. https://doi.org/10.1016/j.ceramint.2010.09.014.
Wiria, F.E., Mian Shyan, J., Lim, P.N., Chung, F., Yeo, J.F., Cao, T. (2010). Printing of Titanium implant prototype. *Mater Design* 31(Suppl. 1), 101–105. https://doi.org/10.1016/j.matdes.2009.12.050.
Xiong, Y., Qian, C., Sun, J. (2012). Fabrication of porous titanium implants by three-dimensional printing and sintering at different temperatures. *Dent. Mater. J.* 31 (5), 815–820. https://doi.org/10.4012/dmj.2012-065.
Yadav, P., Bock, T., Fu, Z., Lorenz, H., Gotman, I., Greil, P., Travitzky, N. (2019). Novel Hybrid Printing of Porous TiC/Ti6Al4V Composites. *Adv. Eng. Mater.* 1900336, 4–11. https://doi.org/10.1002/adem.201900336.
Yan, L., Wu, J., Zhang, L., Liu, X., Zhou, K., Su, B. (2017). Pore structures and mechanical properties of porous titanium scaffolds by bidirectional freeze casting. *Mater. Sci. Eng. C* 75, 335–340. https://doi.org/10.1016/j.msec.2016.12.044.
Yang, G., Xu, B., Lei, X., Wan, H., Yang, B., Liu, D., Wang, Z. (2018). Preparation of porous titanium by direct in-situ reduction of titanium sesquioxide. *Vacuum* 157, 453–457. https://doi.org/10.1016/j.vacuum.2018.09.021.
Yegyan Kumar, A., Wang, J., Bai, Y., Huxtable, S.T., Willams, C.B. (2019). Impacts of process-induced porosity on material properties of copper made by binder jetting additive manufacturing. *Mater. Design* 182, 108001. https://doi.org/10.1016/j.matdes.2019.108001.
Yılmaz, E., Gökçe, A., Findik, F., Gulsoy, H.O., Iyibilgin, O. (2018). Mechanical properties and electrochemical behavior of porous Ti-Nb biomaterials. *J. Mech. Behav. Biomed. Mater* 87, 59–67. https://doi.org/10.1016/j.jmbbm.2018.07.018.
Zadra, M., Casari, F., Girardini, L, Molinari, A. (2008). Microstructure and mechanical properties of cp-titanium produced by spark plasma sintering. *Powder Metall.* 51 (1), 59–65. https://doi.org/10.1179/174329008X277000.
Zhao, D., Han, C., Li, Y., Li, J., Zhou, K., Wei, Q, Liu, J., Shi, Y. (2019). Improvement on mechanical properties and corrosion resistance of titanium-tantalum alloys in-situ fabricated via selective laser melting. *J. Alloys Compd.* 804, 288–298. https://doi.org/10.1016/j.jallcom.2019.06.307.
Ziaee, M., Crane, N.B. (2019). Binder jetting: A review of process, materials, and methods. *Additive Manufacturing* 28, 781–801. https://doi.org/10.1016/j.addma.2019.05.031.